A Robust Unscented Kalman Filter for Intermittent and Featureless Aircraft Sensor Faults

TONGPAN NIE[1], ZIYU DENG[2], YU WANG[1], AND XIANSHENG QIN[2]

[1]The First Aircraft Institute, Aviation Industry Corporation of China, Xi'an 710089, China
[2]School of Mechanical Engineering, Northwestern Polytechnical University, Xi'an 710072, China

Corresponding author: Ziyu Deng (dzy@mail.nwpu.edu.cn)

ABSTRACT Fault tolerance is crucial to reliable state estimations in aircrafts. When time-varying sensor faults are coupled with nonlinear system models, it is non-trivial to robustly recover system states. In this paper, based on an intermittent-measurement unscented Kalman filter (IMUKF), we propose a new state-estimation method by combining the IMUKF with maximum-likelihood estimation and Gaussian mixture reduction. For nonlinear systems under time-varying and featureless sensor faults, the proposed method performs robust estimation without past error history or explicit fault detection, achieving significantly enhanced accuracy under severe conditions. With a nonlinear twin-spool jet engine as the example in simulations, the effectiveness of the proposed method is verified.

INDEX TERMS State estimation, intermittent measurements, fault detection, unscented Kalman filter.

NOMENCLATURE

$^i\boldsymbol{\chi}_k$	The ith sigma point at moment k
δ_{kj}	Kronecker delta
$\boldsymbol{\varepsilon}_k^{(j)}$	Vector of innovation errors in the fault-free sensors under the jth fault hypothesis
$\boldsymbol{\Phi}_k$	Pseudo-measurement matrix, defined as the partial derivative of $\boldsymbol{h}$ with respect to $\boldsymbol{x}$ at $\hat{\boldsymbol{x}}_{k\|k-1}$
$\tilde{\boldsymbol{\Phi}}_k^{(j)}$	Pseudo-measurement matrix for the jth hypothesis
$\gamma_{k,j}$	The jth component of $\boldsymbol{\gamma}_k$
$\boldsymbol{\gamma}_k$	Binary vector describing sensors' fault conditions
ω_i	The ith weight for scattering sigma points. ω_0 is user-specified
ζ_i	Fault-free probability of the ith sensor
$\boldsymbol{A}$	Matrix variable for scattering sigma points
$\boldsymbol{a}_i$	The ith column of matrix $\boldsymbol{A}$
$\boldsymbol{C}_{k\|k-1}$	Approximation of the cross-covariance matrix between the predicted state and measurement vectors for moment k
$\boldsymbol{f}(\cdot)$	Function of nonlinear system dynamics
$\boldsymbol{h}(\cdot)$	Observation function of system state

$\boldsymbol{K}_k^{(j)}$	Kalman gain matrix under the jth hypothesis
$\tilde{\boldsymbol{M}}_k^{(j)}$	Matrix for updating the predicted information matrix
$\boldsymbol{P}_{k\|k}$	Covariance estimation result at moment k
$\boldsymbol{Q}_k$	Process noise covariance matrix at moment k
$\boldsymbol{R}_k$	Measurement noise covariance matrix at moment k
$\tilde{\boldsymbol{R}}_k^{(j)}$	Measurement noise covariance matrix for the jth hypothesis
$\boldsymbol{S}_k^{(j)}$	Covariance matrix of $\boldsymbol{\varepsilon}_k^{(j)}$
$\boldsymbol{u}_k$	Input vector at moment k
$\boldsymbol{v}_k$	Measurement noise vector at moment k
$\boldsymbol{w}_k$	Process noise vector at moment k
$\boldsymbol{x}_k$	System state vector at moment k
$\hat{\boldsymbol{x}}_{k\|k}^{(j)}$	Update state estimation under the jth hypothesis
$\hat{\boldsymbol{x}}_{k\|k-1}$	Predicted state estimation for moment k
$\hat{\boldsymbol{x}}_{k\|k}$	State estimation result at moment k
$\boldsymbol{Y}_{k\|k}^{(j)}$	Updated information matrix under the jth hypothesis
$\boldsymbol{Y}_{k\|k-1}$	Predicted Fisher information matrix for moment k
$\boldsymbol{z}_k$	Vector of sensors' fault-free outputs at moment k
$\hat{\boldsymbol{z}}_{k\|k-1}^{(i)}$	Predicted measurement output corresponding to the ith sigma point for moment k

The associate editor coordinating the review of this manuscript and approving it for publication was Halil Ersin Soken.

$\hat{z}_{k|k-1}$	Predicted measurement output for moment k
$\tilde{z}_k$	True sensors outputs affected by noise and faults at moment k
$E\{\cdot\}$	Expectation operator
n	Dimension of system state
$^i\chi_{k|k-1}$	The ith predicted sigma point for moment k

I. INTRODUCTION

Sensor faults have crucial impacts on the safe operation of aircrafts [1]. Implementing redundant sensors is an effective way of improving safety, but its application is limited by weight and cost constraints. To enhance sensor-system reliability without relying on duplicated sensors, the state-observer-based *analytical redundancy*, which fuses both sensors' measurements and model information, was proposed [2]–[4]. Due to the unknown faults in the sensor systems, classic state observers (e.g., Kalman filter) cannot be directly implemented. Therefore, extensive investigations have been carried out in designing state observers under faulty measurements [5]–[22].

For systems with linear dynamics, many improved versions of the classic Kalman filters (KF) for faulty measurements have been proposed. For example, in the multiple model adaptive estimation (MMAE) methods, multiple classic KFs run in parallel to cover all possible fault hypotheses, and the KF with the minimum innovation error will be selected as the solution to state estimation as well as fault detection and isolation (FDI) [5]–[10]. Another category of approaches is based on adaptive techniques, such as the innovation-based adaptive estimation (IAE) which utilizes the information in the innovation-error sequence [11]–[14], the residual-based adaptive estimation (RAE) that relies on the residual sequence [16], [17], and the robust adaptive KF (RAKF) that implements improved adaption rules for covariance matrices [15], [18]. Since the listed approaches either assume that faults occurred are constant, or rely on the past history of innovation/residual errors for adapting observer parameters, they are not suitable for observing systems with rapidly varying fault conditions. To solve this problem, based on the intermittent-measurement KF (IMKF) formulated in [23], [24], a robust KF for addressing intermittent/permanent faults was proposed in the authors' earlier work [20].

However, as the above methods are all based on KFs, their applications are limited to linear models, which need radical model reductions from real-world system dynamics and significantly sacrifice modeling fidelity. To deal with nonlinear systems, fault-tolerant extended Kalman filters (EKFs) have been applied, e.g., to the state estimation and FDI in the air-data systems [1], [25], [26]. A second-order EKF has also been formulated and evaluated in an atmosphere-reentry problem [27].

As EKFs require systems' Jacobians/Hessians, which may be formidable or inapplicable for many nonlinear systems, researchers developed several estimation methods from the classic unscented Kalman filter (UKF) [28]: For duplicated,

redundant sensors, Bae *et al.* implement parallel UKFs and use the weighted sum of different UKFs' estimations to achieve fault tolerance [29]. For known sensor data absence that simultaneously occurs over the same communication channel, Li and Xia have successfully extended Sinopoli's idea of IMKF [23] to intermittent-measurement UKF [30].

For more general cases with dissimilar types of sensors, unknown and non-synchronously occurred faults, Naderi *et al.* implement multiple parallel UKFs (MM-UKF) to cover all possible fault conditions, whose conditional probabilities are then updated and compared for FDI [31]. Lu *et al.* propose to utilize a time-window of innovation errors to scale the noise covariance matrix, arriving at the adaptive fading UKF (AFUKF), whose individual channels are triggered if the corresponding innovation errors exceed some user-specified thresholds [19]. But similar to the RAKF [15], [15], [18], [18], the parameter-adaption process slows down the response to rapidly varying fault conditions, resulting in significant performance sacrifice [20].

The introduced methods have been successfully applied to a large number of state-estimation problems under sensor faults. But when performing state estimations for nonlinear systems under both intermittent and permanent sensor faults, the following problems are encountered:

- The KF-based methods, such as MMAE, IAE, RAE, RAKF, and IMKF, etc., do not fit nonlinear systems, whereas the EKF-based methods need Jacobian/Hessian computations, and can only be applied to slightly nonlinear systems [28];
- For nonlinear systems, the implementation of UKF-based methods are constrained to particular situations: E.g., duplicated sensors, known fault conditions, or slowly varying faults. It is still a challenge to apply UKF to systems with intermittent and time-varying faults. In contrast, sensors in aircrafts cover diversified types, and their faults can be intermittent and quickly changing.

To relax the constraints on nonlinear estimations and fault assumptions, in this paper, by the approximations of the information and cross-covariance matrices, a pseudo-measurement matrix is formulated, enabling the use of IMUKF under intermittent faults. Besides, the Gaussian mixture-model is used to merge the multiple estimation results under different fault hypothesis, arriving at the presented method. In particular, it leads to the following improvements:

- A novel robust IMUKF is formulated. The robust IMUKF does not rely on the slowly-varying or knowing-fault assumptions, leading to the expanded application scenarios and enhanced accuracy under rapidly-varying sensor faults;
- The estimations under different fault conditions are merged automatically in maximum-likelihood manner without referring to manually-specified FDIs, allowing fast implementations of the algorithm in various scenarios.
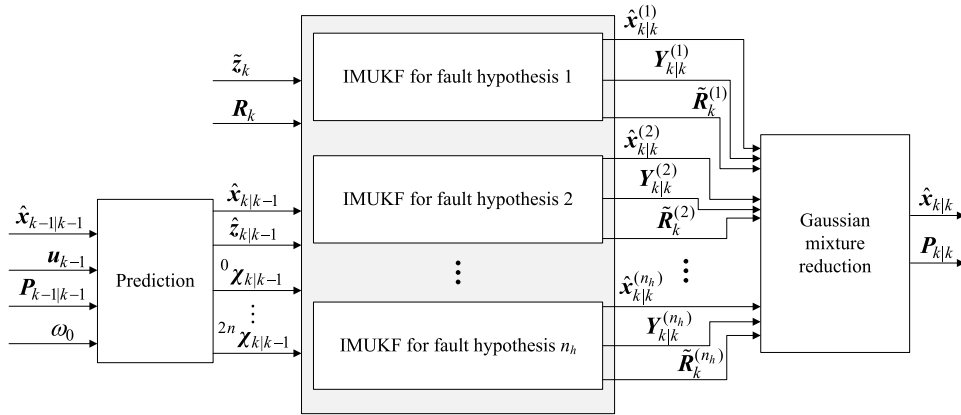
FIGURE 1. Data-flow diagram of the proposed method.

The coordination of IMUKF and maximum-likelihood FDI is verified in simulations with a nonlinear jet engine example, and the estimation accuracy is compared with those of the state-of-the-art methods.

This paper is organized as follows: The problem of state estimation for nonlinear system under sensor faults is introduced in Section II. The proposed method is presented in detail in Section III. In Section IV, by using a nonlinear jet-engine model as an example, the performance of the proposed method is evaluated and compared with other state-of-the-art methods. Conclusions are given in Section V.

II. PROBLEM FORMULATION

For a nonlinear, discrete system, we assume $x_k \in \mathbb{R}^n$ is the vector of system state at moment k, $u_k \in \mathbb{R}^r$ is the input vector, and $z_k \in \mathbb{R}^m$ denotes the vector of sensors' fault-free outputs, then the system's nonlinear dynamics are given by

$$x_{k+1} = f(x_k, u_k) + w_k$$
$$z_k = h(x_k) + v_k, \tag{1}$$

where f and h are nonlinear functions describing the state-transition and observation processes, respectively. $w_k \in \mathbb{R}^n$ and $v_k \in \mathbb{R}^m$ are the process and measurement noises at moment k, respectively. We assume w_k and v_k are both independent and zero-mean, satisfying

$$E\{w_k w_j^T\} = Q_k \delta_{kj}$$
$$E\{v_k v_j^T\} = R_k \delta_{kj}, \tag{2}$$

where $E\{\cdot\}$ is the expectation operator, δ_{kj} is the Kronecker delta, and Q_k and R_k are the covariance matrices for process and measurement noises, respectively.

We assume that sensor faults can occur, intermittently or permanently, in any single or combination of sensors. An m-dimensional binary vector

$$\gamma_k = [\gamma_{k,1}, \gamma_{k,2}, \ldots, \gamma_{k,m}]^T \tag{3}$$

is used to describe sensors' fault conditions at moment k, where 1 means that the sensor is working properly, and 0 indicates a sensor failure. γ_k is unknown to the observers, but

we assume that each sensor has an expected value of failure rate, which is derived from the sensor's MTBF (mean time between failure). Thus the fault-free probability of the ith sensor is given by

$$\zeta_i = E(\gamma_{k,i}), \quad \forall i = 1, 2, \ldots, m \tag{4}$$

Note that in practice ζ_i are rough estimates and may be deviated from the true values (see Table 1).

When a sensor is without fault, we assume that its measurement conforms with the model in (1). Otherwise, the faulty sensor is assumed to feedback erroneous and featureless values that could span the admissible range of its output. Let $\tilde{z}_1$, $\tilde{z}_2, \ldots, \tilde{z}_k$ be the measurements affected by both noises and faults. We aim to recover the state of the nonlinear system (1) from $\tilde{z}_1, \tilde{z}_2, \ldots, \tilde{z}_k$, and the estimation method is presented in the following section.

III. PROPOSED METHOD

An overview of the proposed method is summarized in the data-flow diagram in Fig. 1. The inputs of the diagram are the estimated state $\hat{x}_{k-1|k-1}$ and covariance $P_{k-1|k-1}$ for moment $k-1$. The outputs are $\hat{x}_{k|k}$ and $P_{k|k}$, which at moment $k+1$ will become the input for the next iteration. The three blocks relating the input and output are namely prediction, IMUKF and Gaussian mixture reduction, which are detailed below.

A. PREDICTION

For nonlinear systems, the first step of prediction is the generation of $2n+1$ *sigma points* ${}^0\chi_{k-1}, {}^1\chi_{k-1}, \ldots, {}^{2n}\chi_{k-1}$, where n is the dimension of system state. Let $-1 < \omega_0 < 1$ be a user-specified weight, which controls the distance between ${}^1\chi_{k-1}, \ldots, {}^{2n}\chi_{k-1}$ and the origin ${}^0\chi_{k-1}$. The sigma points' weights and locations are given as [28]:

$$\omega_i = \frac{1 - \omega_0}{2n}, \quad \forall i = 1, 2, \ldots, 2n$$
$${}^0\chi_{k-1} = \hat{x}_{k-1|k-1}$$
$${}^i\chi_{k-1} = \begin{cases} {}^0\chi_{k-1} - a_i, & i = 1, 2, \ldots, n, \\ {}^0\chi_{k-1} + a_i, & i = n+1, n+2, \ldots, 2n, \end{cases} \tag{5}$$

where a_i is the *i*th column of matrix A, which is defined as

$$A = \sqrt{\frac{n}{1-\omega_0}P_{k-1|k-1}}. \tag{6}$$

Given $^0\chi_{k-1}$, $^1\chi_{k-1}, \ldots, ^{2n}\chi_{k-1}$ with weights ω_0, $\omega_1, \ldots, \omega_{2n}$, the new location of each sigma point is predicted using the nonlinear model and the input at moment $k-1$:

$$^i\chi_{k|k-1} = f(^i\chi_{k-1}, u_{k-1}). \tag{7}$$

The system's state and measurements are predicted by

$$\hat{x}_{k|k-1} = \sum_{i=0}^{2n} \omega_i {}^i\chi_{k|k-1},$$

$$\hat{z}_{k|k-1} = \sum_{i=0}^{2n} \omega_i \hat{z}_{k|k-1}^{(i)}, \tag{8}$$

where

$$\hat{z}_{k|k-1}^{(i)} = h(^i\chi_{k|k-1}). \tag{9}$$

B. IMUKF UNDER A SPECIFIC FAULT HYPOTHESIS

To facilitate the fusion of measurements from multiple sensors, we implement the Fisher information matrix $Y_{k|k-1}$ [32] and approximate it by

$$Y_{k|k-1} \approx \left(\sum_{i=0}^{2n} \omega_i \left({}^i\chi_{k|k-1} - \hat{x}_{k|k-1} \right) \right.$$

$$\left. \times \left({}^i\chi_{k|k-1} - \hat{x}_{k|k-1} \right)^T \right)^{-1}. \tag{10}$$

The cross-covariance matrix between the predicted state and measurements is approximated by

$$C_{k|k-1} \approx \sum_{i=0}^{2n} \omega_i \left({}^i\chi_{k|k-1} - \hat{x}_{k|k-1} \right) \left(\hat{z}_{k|k-1}^{(i)} - \hat{z}_{k|k-1} \right)^T. \tag{11}$$

Then the matrices $Y_{k|k-1}$ and $C_{k|k-1}$ are used to formulate the pseudo-measurement matrix of $h(x)$ as

$$\Phi_k = Y_{k|k-1} C_{k|k-1} \approx \left. \frac{\partial h}{\partial x} \right|_{\hat{x}_{k|k-1}}. \tag{12}$$

As the true γ_k in (3) is unknown, the UKF has to cover all possible fault conditions. Let $\gamma^{(j)}$ be the *j*th fault hypothesis, i.e., it denotes the *m*-dimensional binary representation of *j*, a set of matrices can be defined as

$$\tilde{\Phi}_k^{(j)} = \mathrm{diag}(\gamma^{(j)})\Phi_k,$$

$$\tilde{R}_k^{(j)} = \mathrm{diag}(\gamma^{(j)})R_k,$$

$$\tilde{M}_k^{(j)} = \sum_{i=1}^m \frac{\gamma_{k,i}}{r_i} {}^i\phi_k {}^i\phi_k^T, \tag{13}$$

r_i is the *i*th-row, *i*th-column entry of R_k, and $^i\phi_k$ is the *i*th column of Φ_k^T in (12).

Given the real measurements $\tilde{z}_k$ and with the above formulations, the updated state estimation under the *j*th fault hypothesis is calculated by the following rules:

$$Y_{k|k}^{(j)} = Y_{k|k-1} + \tilde{M}_k^{(j)},$$

$$K_k^{(j)} = Y_{k|k}^{(j)}{}^{-1} (\tilde{\Phi}_k^{(j)})^T (\tilde{R}_k^{(j)})^\dagger,$$

$$\hat{x}_{k|k}^{(j)} = \hat{x}_{k|k-1} + K_k^{(j)} \left(\tilde{z}_k - \hat{z}_{k|k-1} \right), \tag{14}$$

where $(\cdot)^\dagger$ stands for the left pseudoinverse of a matrix.

C. GAUSSIAN MIXTURE REDUCTION

To select the subset of sensors that have no fault at moment k, we form a "selection matrix" G_j by removing the all-zero rows of $\mathrm{diag}(\gamma^{(j)})$, while the left rows indicate those properly working sensors. Then the vector of valid (not affected by sensor faults) innovation errors are given by

$$\varepsilon_k^{(j)} = G_j \left(\tilde{z}_k - \hat{z}_{k|k-1} \right), \tag{15}$$

whose covariance matrix is

$$S_k^{(j)} = G_j \left(\Phi_k Y_{k|k-1}^{-1} \Phi_k^T + \tilde{R}_k^{(j)} \right) G_j^T. \tag{16}$$

With $S_k^{(j)}$ and each sensor's fault-free probability ζ_i in (4), the steps of obtaining the conditional probability $P(\gamma^{(j)}|\varepsilon_k^{(j)})$ have been presented in [20] and are skipped here. The results of Gaussian mixture reduction are

$$\hat{x}_{k|k} = \sum_{j=1}^{2^m-1} P(\gamma^{(j)}|\varepsilon_k^{(j)})\hat{x}_{k|k}^{(j)}, \tag{17}$$

$$P_{k|k} = \sum_{j=1}^{2^m-1} P(\gamma^{(j)}|\varepsilon_k^{(j)})T^{(j)}, \tag{18}$$

where

$$T^{(j)} = \left(Y_{k|k}^{(j)} \right)^{-1} + \left(\hat{x}_{k|k}^{(j)} - \hat{x}_{k|k} \right) \left(\hat{x}_{k|k}^{(j)} - \hat{x}_{k|k} \right)^T. \tag{19}$$

The above formulations fully describe the process between the inputs and outputs in Fig. 1. For continuously estimating system states in real time, this process is iteratively performed with a user-specified stop condition. To deal with the rare cases where all sensors fail simultaneously, a variation-limit threshold $\bar{\Delta}$ is specified on $\|\hat{x}_{k|k} - \hat{x}_{k-1|k-1}\|_2$, whose upper bound can be determined beforehand from the characteristics of the monitored system [20]. Finally, the proposed method is summarized in Algorithm 1.

IV. SIMULATION

A. NONLINEAR SYSTEM EXAMPLE

A simplified nonlinear jet-engine model in [33] is implemented to validate the proposed method. In the jet-engine model, the system state $x = [x_1, x_2, x_3]^T$ is the normalized change of the low-pressure compressor speed, high-pressure compressor speed, and burner fuel flow, respectively. $z \in \mathbb{R}^6$ contains the measurements from six sensors. The input u is the normalized change of the commanded fuel flow. Assuming the sampling period is 0.01 s, the engine's

Algorithm 1 The Proposed Robust UKF Method

Input: System model $f(\cdot)$, $h(\cdot)$, process and measurement noise covariances Q and R, sensors' fault-free probabilities $\zeta_1, \ldots, \zeta_m$, inputs $u_1, u_2, \ldots$, etc., sigma-point weight ω_0, measurements $\tilde{z}_1, \tilde{z}_2, \tilde{z}_3, \ldots$, etc., state-variation threshold $\bar{\Delta}$, and iteration stop condition z_{stop}.

Output: State estimations $\hat{x}_{1|1}, \hat{x}_{2|2}, \hat{x}_{3|3}, \ldots$, etc., and estimation covariances $P_{1|1}, P_{2|2}, P_{3|3}, \ldots$, etc.

1 Initialize $\hat{x}_{0|0}$ and covariance $P_{0|0}$, $k \leftarrow 0$;
2 **while** $z_{stop} \neq$ `true` **do**
3      $k \leftarrow k + 1$;
4      $\hat{x}_{k|k-1} \leftarrow 0$;
5      $\hat{z}_{k|k-1} \leftarrow 0$;
6   **for** $i = 0$ to $2n$ **do**
7   Generate the ith sigma point ${}^i\chi_{k-1}$ with weight ω_i, using (5) and (6), with the given ω_0 and the previously obtained $P_{k-1|k-1}$;
8   Obtain ${}^i\chi_{k|k-1}, \hat{z}_{k|k-1}^{(i)}, \hat{x}_{k|k-1}$, and $\hat{z}_{k|k-1}$ using (7) and (8), with ${}^i\chi_{k|k-1}, u_{k-1}, \omega_i$, and the system model;
9   **end**
10   Get $Y_{k|k-1}$ and $C_{k|k-1}$ using (10) and (11);
11      $\Phi_k \leftarrow Y_{k|k-1}C_{k|k-1}$;
12   **for** $j = 1$ to $2^m - 1$ **do**
13   Calculate $\tilde{\Phi}_k^{(j)}, \tilde{R}_k^{(j)}$, and $\tilde{M}_k^{(j)}$ using (13);
14   Update $Y_{k|k}^{(j)}$ and $\hat{x}_{k|k}^{(j)}$ using (14) with the real measurement $\tilde{z}_k$;
15   Compute the valid innovation error $\varepsilon_k^{(j)}$ and its covariance $S_k^{(j)}$ using (15) and (16);
16   **end**
17      $\hat{x}_{k|k} \leftarrow 0$;
18   **for** $j = 1$ to $2^m - 1$ **do**
19   Compute $P(\gamma^{(j)}|\varepsilon_k^{(j)})$ using (11)–(14) in [20];
20          $\hat{x}_{k|k} \leftarrow \hat{x}_{k|k} + P(\gamma^{(j)}|\varepsilon_k^{(j)})\hat{x}_{k|k}^{(j)}$;
21   **end**
22   **if** $\|\hat{x}_{k|k} - \hat{x}_{k-1|k-1}\|_2 > \bar{\Delta}$ **then**
23          $\hat{x}_{k|k} \leftarrow \hat{x}_{k|k-1}$;
24          $P_{k|k} \leftarrow Y_{k|k-1}^{-1}$;
25   **Continue**;
26   **end**
27      $P_{k|k} \leftarrow 0$;
28   **for** $j = 1$ to $2^m - 1$ **do**
29   Compute $T^{(j)}$ using (19) with $Y_{k|k}^{(j)}, \hat{x}_{k|k}^{(j)}$, and $\hat{x}_{k|k}$;
30          $P_{k|k} \leftarrow P_{k|k} + P(\gamma^{(j)}|\varepsilon_k^{(j)})T^{(j)}$;
31   **end**
32 **end**

nonlinear dynamics is described by
$$x_{k+1} = Q_{\text{sys}}q(x_k) + A_{\text{sys}}x_k + B_{\text{sys}}u_k,$$
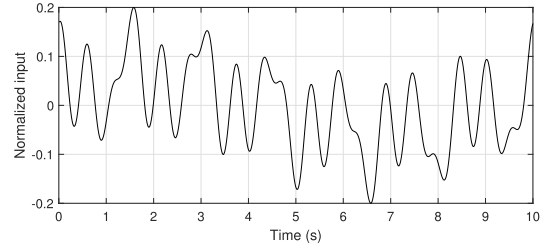$$z_k = C_{\text{sys}}x_k, \qquad (20)$$

FIGURE 2. Normalized input u (commanded fuel flow) to system (20) in the simulation.

TABLE 1. Fault conditions of the outputs in the simulation.

Sensor index	True ζ	Guessed ζ
1	0.97	0.95
2	0.96	0.95
3	0.96	0.95
4	0.94	0.90
5	0.93	0.90
6	0.92	0.90

where $q(x)$ includes the nonlinear terms of x:
$$q(x) = [x_1^2, x_2^2, x_3^2, x_1x_2, x_1x_3, x_2x_3]^T, \qquad (21)$$

and

$$Q_{\text{sys}}^T = \begin{bmatrix} 1.3293 & 5.6812 & 0 \\ 3.4440 & -0.5281 & 0 \\ 0.1375 & -0.3385 & 0 \\ -5.1304 & -1.6193 & 0 \\ -1.7826 & 0.5229 & 0 \\ -1.8719 & 0 & 0 \end{bmatrix} \times 10^{-2},$$

$$A_{\text{sys}} = \begin{bmatrix} 0.9844 & 0.0069 & 0.0040 \\ 0.0026 & 0.9778 & 0.0022 \\ 0 & 0 & 0.9 \end{bmatrix},$$

$$B_{\text{sys}} = [0, 0, 0.1]^T,$$

$$C_{\text{sys}} = \begin{bmatrix} I_{3\times3} \\ 0.5511 & 0.1332 & 0.3060 \\ 0.5522 & 0.1353 & 0.3291 \\ -0.2569 & -0.2363 & 0.6120 \end{bmatrix}.$$

Both the process and measurement noises in this example are assumed to be independent and Gaussian. The standard deviations of the process noise are assumed to be $[2e{-}4, 2e{-}4, 2e{-}4]^T$, and the standard deviations of the measurement noise are $[0.001, 0.001, 0.01, 0.02, 0.02, 0.03]^T$.

B. SIMULATION SETTINGS
This simulation time was set to 10 s. The input signal (commanded fuel flow) was randomly generated using sums of a set of sinusoids and is shown in Fig. 2.

The six sensors are assumed to have independently occurred faults, whose true fault-free probabilities are given in Table 1. Besides, we assume that the system designer do not have the accurate values of these probabilities, whose rough guesses are also listed in the rightmost column of Table 1.

Aside from the randomly and intermittently occurred faults, a set of permanent or temporary faults in the sensors were also introduced as follows:

- A permanent fault occurred in sensor 2 from $t = 6$ s till the end of the simulation;
- Three faults occurred in sensors 1, 3 and 6 simultaneously from $t = 7$ s. The fault in sensor 1 disappeared at $t = 8$ s, whereas the faults in sensors 3 and 6 continued to the end of the simulation.

The true initial state of the system is set to $\boldsymbol{x}_0 = [0, 0, 0]^T$, while the initial estimated state is assumed to be $\hat{\boldsymbol{x}}_{0|0} = [0.001, 0.001, 0.001]^T$. To provide an initial covariance matrix, we assume that the initial estimations of compressor speeds and fuel flow have independent errors, with standard deviations as 5% and 10% of their working ranges, respectively, corresponding to $\boldsymbol{P}_{0|0} = \mathrm{diag}([0.05^2, 0.05^2, 0.1^2]^T)$. The state-variation limit $\bar{\Delta}$ is set to 0.005, utilizing the system property that the magnitude of engine state change does exceed 50% (of the working range) within 1 s.

Since the estimation error $\boldsymbol{e}_k = \hat{\boldsymbol{x}}_{k|k} - \boldsymbol{x}_k$ comes from the error components with different ranges, to quantify the estimation error on the same basis, a normalized estimation error $\bar{\boldsymbol{e}}_k \in \mathbb{R}^3$ is defined as follows:

$$\bar{\boldsymbol{e}}_k = \mathrm{diag}([\theta_1, \theta_2, \theta_3])^{-1} \boldsymbol{e}_k, \tag{22}$$

where θ_j is the peak-to-peak value of the jth state component, i.e.,

$$\theta_j = \max_{k=1}^{N} x_{j,k} - \min_{k=1}^{N} x_{j,k}, \quad \forall j = 1, 2, 3,$$

with $N = 1000$ is the number of sampling moments in the simulation. With the normalized estimation error $\bar{\boldsymbol{e}}_k$, two scalar measures of the mean and maximum estimation errors are defined as

$$e_{\mathrm{mean}} = \sum_{k=1}^{N} \|\bar{\boldsymbol{e}}_k\| / N,$$

$$e_{\mathrm{max}} = \max_{k=1,2,\dots,N} \|\bar{\boldsymbol{e}}_k\|. \tag{23}$$

Besides the mean estimation error, to quantify the distribution of $\bar{\boldsymbol{e}}_k$, we introduce another measure $v_{95\%}$, which corresponds to the volume of the ellipsoid that contains $\bar{\boldsymbol{e}}_k$ with 95% confidence. The ellipsoid's volume is computed by

$$v_{95\%} = \frac{4}{3}\pi\sqrt{7.815^3 \lambda_1 \lambda_2 \lambda_3}, \tag{24}$$

where λ_1, λ_2, and λ_3 are the three eigenvalues of the covariance matrix of $\bar{\boldsymbol{e}}_1, \bar{\boldsymbol{e}}_2, \dots, \bar{\boldsymbol{e}}_N$. The value 7.815 corresponds to the critical value of the three degree-of-freedom χ^2 distribution with over 95% cumulative probability.

C. SIMULATION RESULTS

With the initial conditions, inputs, and fault probabilities given above, simulations were performed for the nonlinear system in (20). The sensors' measurements are shown in Fig. 3, which includes six sensors' signals that are severely affected by noises and faults. Besides the intermittent faults (peaks in the signals), we assume that permanent faults also occur on four of the six sensor, as indicated by the vertical lines in Fig. 3.
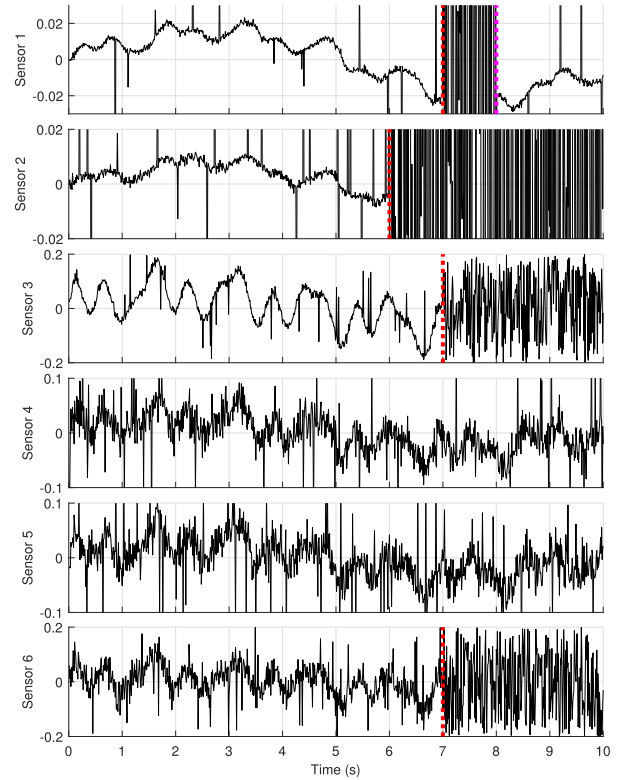

FIGURE 3. Sensors' measurements subject to noises and faults. The crude peaks in the signals correspond to the intermittent faults. The red and magenta vertical dashed lines denote the moments of entering and leaving the long-term faults, respectively.
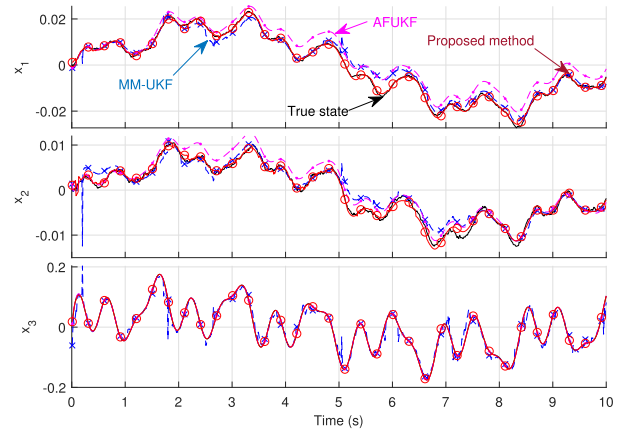

FIGURE 4. State-estimation results using MM-UKF, AFUKF, and the proposed method. The black solid curve corresponds to the true system state. The blue dashed (with "x" markers), magenta dashed (with "·" markers), and red solid (with "o" markers) curves correspond to the results of MM-UKF, AFUKF, and the proposed method, respectively.

State estimations were performed using the proposed method and parameters given in Section IV-B. The estimation result is shown in Fig. 4.

Despite the largely disturbed measurements in Fig. 3, the state-estimation result in Fig. 4 suggests that the system
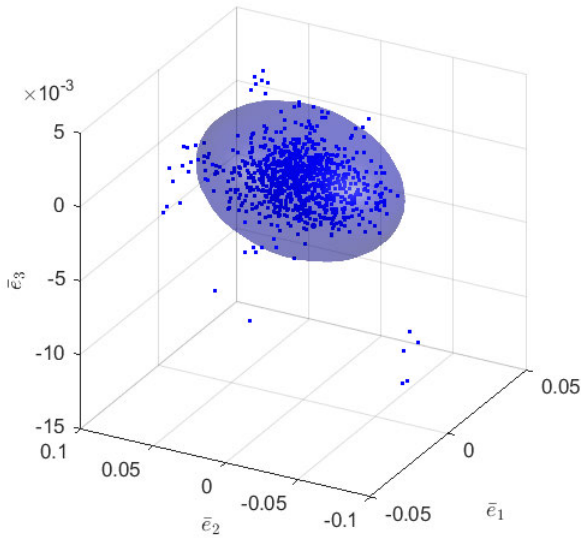
FIGURE 5. Distribution of the normalized estimation errors. The ellipse shows the error-distribution region with 95% confidence.

FIGURE 6. Comparing the normalized estimation errors of three methods. The green, blue, and red dots correspond to the estimation errors of the MM-UKF, AFUKF, and the proposed methods, respectively. The green, blue, and red ellipsoids stand for the 95%-confidence regions for the MM-UKF, AFUKF, and the proposed methods, respectively.

states are recovered successfully (as is compared with the true state values in the same figure).

To quantify the estimation accuracy in the three-dimensional state space, the normalized estimation error $\bar{e}$ is implemented and visualized in Fig. 5, which suggests that 95% estimation errors fall inside the three-dimensional ellipsoid with major axes lengths as 0.0738, 0.0308, and 0.0044, respectively.

The volume of the confidence ellipsoid is 4.19×10^{-5}. The mean error of estimation, defined as e_{mean} in (23), is obtained as 0.0238, meaning that the estimation error is expected to be 2.38% with respect to the signals' peak-to-peak values. The above results on error distributions further validate the accuracy of the proposed method against unknown and intermittent sensor faults.

Besides the estimation accuracy, the algorithm's timing and memory performances have also been tested in benchmarks. The proposed method takes 88803 floating point operations for each sampling moment, and occupies roughly 1024 kB memory. These resource requirements can be met by many typical embedded systems (e.g., ARM Cortex M7 with roughly 15 MFLOPS capability and 16 MB memory). On a x86-AMD64 computer with six-core CPU (Intel i7-8750H) at 2.20 GHz clock rate and 16 GB memory, the computation time for each iteration is 0.381 ms, which is sufficiently shorter than the 10 ms observer period. In addition, the computation process for each independent fault hypothesis in (13)–(16) is parallelized for further improved efficiency.

D. METHOD COMPARISON

Besides the proposed method, the following state-of-the-art methods have also been tested in simulations:

- Multiple parallel UKFs (MM-UKF): Multiple UKFs are running in parallel for all possible fault hypotheses.
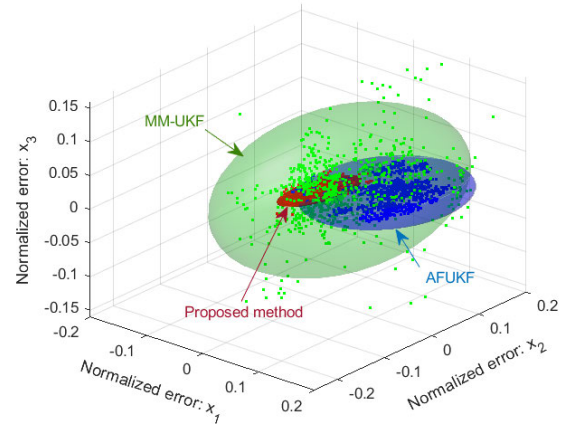
The conditional probability of each hypothesis is computed using the corresponding innovation error. The state/covariance update follows the hypothesis that owns the maximum conditional probability [31];

- Adaptive fading UKF (AFUKF): With a time-window of innovation errors, threshold-based FDI is performed in each sensor channel. For the faulty sensors, the measurement-noise covariance $\boldsymbol{R}$ is adaptively modified for realizing fault-tolerant estimations [19]. In the simulation, the time-window length is 100, and the FDI thresholds for the six sensors are set to be three times of their standard deviations. In this example, the result of AFUKF demonstrated no sensitivity to the above parameters, while a set of parameter-tuning tests were still performed to find the above listed parameter sets.

Using the same inputs and measurements, performances of the above methods are examined in simulations. A comparison of the estimation errors of the discussed methods are visualized in Fig. 6:

1) Graphically, for the proposed method, the volume of its 95% confidence ellipsoid of the estimation errors is apparently smaller than those of the MM-UKF and AFUKF;

2) A quantitative comparison of the three methods' accuracies is given in Table 2, including specifications such as mean errors, maximum errors, and ellipsoid volumes. It can be observed that the proposed method leads to significant error-reduction in the listed specifications.

The different confidence ellipses in Fig. 6 graphically show that, compared with the MM-UKF and AFUKF, the proposed method has significantly reduced the estimation errors. More accuracy measures and computation costs of the three methods are listed in Table 2.

TABLE 2. Comparison of the estimation errors and computation times of three methods.

|	MM-UKF	AFUKF	Proposed method
e_{mean}	0.0733	0.1043	0.0238
e_{max}	0.7200	0.1850	0.0910
$v_{95\%}$	9.0441×10^{-3}	2.8680×10^{-4}	4.1877×10^{-5}
Time cost	0.574 ms	0.528 ms	0.381 ms

- We can see that when the fault conditions are rapidly time-varying, the MM-UKF has large estimation errors. The reason is that in MM-UKF, the computation of conditional probabilities of fault hypotheses relies on the past results. This design is very efficient for permanent faults, but does not fit the simulated scenario;
- The AFUKF does not assume the constant-fault condition, however, the covariance-adaption process of the AFUKF introduces "lags" to rapidly changing fault conditions, making it more suitable for slowly varying faults (e.g., drifts of sensors' offsets);
- As IMUKF allows the instantaneous handling of intermittent measurements, and Gaussian mixture reduction allows the FDI to work without assumption on the past error history, the proposed method leads to better estimation accuracy under unknown and intermittent sensor faults. Besides, compared with MM-UKF and AFUKF, the proposed method leads to no increase in the computation cost, hence is suitable to be implemented in real-time estimation tasks.

Compared with the two state-of-the-art methods, the proposed method results in 67.5% and 77.2% reduction in the mean normalized errors, respectively. The confidence region has also been reduced by 99.5% (MM-UKF) and 85.4% (AFUKF), respectively. These results verify the the accuracy improvements of the proposed method.

E. ESTIMATION ACCURACIES UNDER NON-GAUSSIAN MEASUREMENT NOISES

In practice, the measurement noises are usually non-Gaussian, and their effects on estimation accuracies should be evaluated. Therefore, in our simulations, besides the Gaussian noise (with corresponding results presented above), we also considered two other typical types of heavy-tail, non-Gaussian noises, namely the Laplace noise and Cauchy noise, which in the simulations are assumed to be zero-mean, and are scaled to have the same standard deviations as the Gaussian case. The rationale of scaling is not only for a "fair" comparison, but also because that for avionics, the sensors should be provided with their standard deviations (obtained statistically), even if their noises are not Gaussian. A comparison of the estimation results, using the proposed method under different measurement noises, is shown in Fig. 7, and the estimation errors are quantified by the measures in (23) and (24), and listed in Table 3.

According to the above comparison, no evident accuracy deterioration is observed in the cases of Laplace and Cauchy noises. The estimation errors do not demonstrate significant sensitivity to non-Gaussian measurement noises, and can be
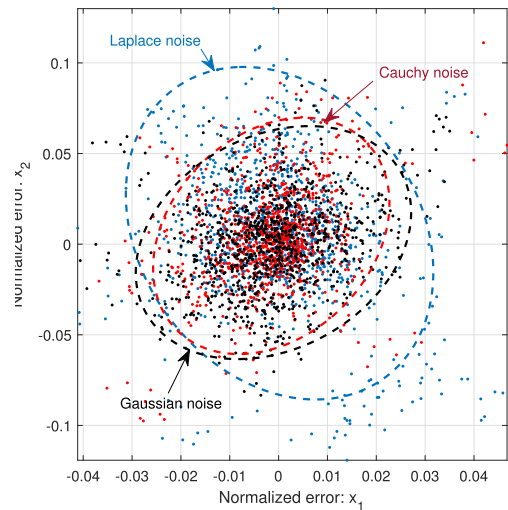
(a) Top view
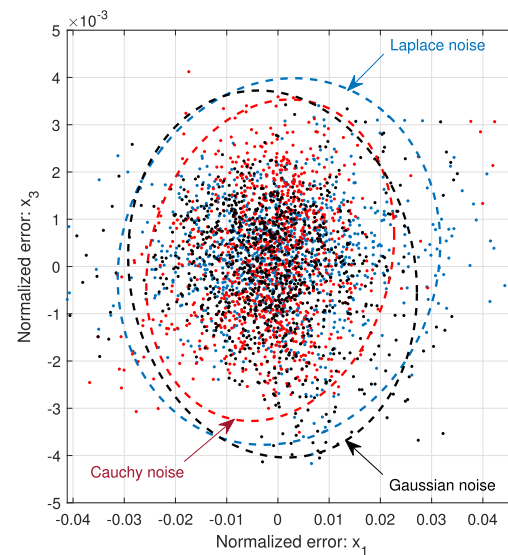
(b) Front view

FIGURE 7. Comparing the normalized estimation errors under different noise types. The blue, red and black dots correspond to the estimation errors under Laplace, Cauchy and Gaussian noises, respectively. The blue, red and black ellipses stand for the 95%-confidence regions corresponding to the Laplace, Cauchy and Gaussian noises, respectively.

TABLE 3. Comparison of the accuracies under different types of noises.

	Laplace	Cauchy	Gaussian
e_{mean}	0.0314	0.0222	0.0238
e_{max}	0.1299	0.1188	0.0910
$v_{95\%}$	6.6965×10^{-5}	3.1479×10^{-5}	4.1877×10^{-5}

employed in practical cases where most noises are not strictly Gaussian.

V. CONCLUSION

Aircrafts are equipped with various types of sensors, which are subject to both permanent and intermittent faults under severe flight conditions. When the monitored system has nonlinear dynamics, it is non-trivial to design a

fault-tolerant observer to recover system states. In this paper, based on the formulation of an IMUKF, we implement maximum-likelihood estimation and Gaussian mixture reduction, and propose a robust filter that fits nonlinear estimations with unknown and featureless faults, which could either be permanent or intermittent. Using a nonlinear engine model as the simulation example, we test the proposed method and compare its performance with those of two state-of-the-art methods, namely MM-UKF and AFUKF. The simulation results verify that the proposed method leads to significant enhancement of the estimation accuracy.

The present work can be improved in many ways. For example, more objective functions for optimizing the Kalman gain can be analyzed and tested to account for more general, non-Gaussian measurement noises [34], [35]. Techniques such the H_∞ and peak-to-peak filters can be implemented to weaken the statistical assumptions on the measurement noises [36], [37]. In addition, besides sensors' faults, the proposed method can be extended to deal with actuators' faults. These issues are to be explored in the future work.

REFERENCES

[1] A. Ansari and D. S. Bernstein, "Aircraft sensor fault detection using state and input estimation," in *Proc. Amer. Control Conf. (ACC)*, Jul. 2016, pp. 5951–5956.

[2] P. M. Frank, "Fault diagnosis in dynamic systems using analytical and knowledge-based redundancy: A survey and some new results," *Automatica*, vol. 26, no. 3, pp. 459–474, 1990.

[3] R. J. Patton, "Fault detection and diagnosis in aerospace systems using analytical redundancy," *Comput. Control Eng. J.*, vol. 2, no. 3, pp. 127–136, May 1991.

[4] R. J. Patton and J. Chen, "Robust fault detection of jet engine sensor systems using eigenstructure assignment," *J. Guid., Control, Dyn.*, vol. 15, no. 6, pp. 1491–1497, Nov. 1992.

[5] D. Magill, "Optimal adaptive estimation of sampled stochastic processes," *IEEE Trans. Autom. Control*, vol. AC-10, no. 4, pp. 434–439, Oct. 1965.

[6] R. A. Gray and P. S. Maybeck, "An integrated GPS/INS/baro and radar altimeter system for aircraft precision approach landings," in *Proc. IEEE Nat. Aerosp. Electron. Conf. (NAECON)*, vol. 1, May 1995, pp. 161–168.

[7] Y. Zhang and X. R. Li, "Detection and diagnosis of sensor and actuator failures using IMM estimator," *IEEE Trans. Aerosp. Electron. Syst.*, vol. 34, no. 4, pp. 1293–1313, Oct. 1998.

[8] P. S. Maybeck, "Multiple model adaptive algorithms for detecting and compensating sensor and actuator/surface failures in aircraft flight control systems," *Int. J. Robust Nonlinear Control*, vol. 9, no. 14, pp. 1051–1070, Dec. 1999.

[9] T. Kobayashi and D. L. Simon, "Aircraft engine sensor-actuator-component fault diagnosis using a bank of Kalman filters," NASA, Washington, DC, USA, Tech. Rep. NASA/CR–2003-212298, 2003, p. 40.

[10] C. D. Ormsby, J. F. Raquet, and P. S. Maybeck, "A new generalized residual multiple model adaptive estimator of parameters and states," *Math. Comput. Model.*, vol. 43, nos. 9–10, pp. 1092–1113, May 2006.

[11] R. Mehra, "On the identification of variances and adaptive Kalman filtering," *IEEE Trans. Autom. Control*, vol. AC-15, no. 2, pp. 175–184, Apr. 1970.

[12] R. Mehra, "On-line identification of linear dynamic systems with applications to Kalman filtering," *IEEE Trans. Autom. Control*, vol. AC-16, no. 1, pp. 12–21, Feb. 1971.

[13] T. Kailath, "A note on least-squares estimation by the innovations method," in *Proc. IEEE Conf. Decis. Control*, Dec. 1971, pp. 407–411.

[14] P. S. Maybeck, *Stochastic Models, Estimation, and Control*, vols. 1–2. New York, NY, USA: Academic, 1982.

[15] C. Hajiyev and F. Caliskan, "Sensor/actuator fault diagnosis based on statistical analysis of innovation sequence and robust Kalman filtering," *Aerosp. Sci. Technol.*, vol. 4, no. 6, pp. 415–422, Sep. 2000.

[16] A. H. Mohamed and K. P. Schwarz, "Adaptive Kalman filtering for INS/GPS," *J. Geodesy*, vol. 73, no. 4, pp. 193–203, May 1999.

[17] J. Wang, M. Stewart, and M. Tsakiri, "Adaptive Kalman filtering for integration of GPS with glonass and ins," in *Geodesy Beyond 2000*. Springer, 2000, pp. 325–330.

[18] C. Hajiyev and H. E. Soken, "Robust adaptive Kalman filter for estimation of UAV dynamics in the presence of sensor/actuator faults," *Aerosp. Sci. Technol.*, vol. 28, no. 1, pp. 376–383, Jul. 2013.

[19] P. Lu, L. Van Eykeren, E.-J. Van Kampen, Q. P. Chu, and B. Yu, "Adaptive hybrid unscented Kalman filter for aircraft sensor fault detection, isolation and reconstruction," in *Proc. AIAA Guid., Navigat., Control Conf.* Reston, VA, USA: American Institute Aeronautics Astronautics, Jan. 2014, p. 1145.

[20] H. Wang, D. Liu, T. Chen, and X. Qin, "A robust state estimation method for unknown, time-varying and featureless aircraft sensor failures," *IEEE Access*, vol. 8, pp. 118125–118134, 2020.

[21] L. Ma, N. Xu, X. Huo, and X. Zhao, "Adaptive finite-time output-feedback control design for switched pure-feedback nonlinear systems with average dwell time," *Nonlinear Anal., Hybrid Syst.*, vol. 37, Aug. 2020, Art. no. 100908.

[22] Y. Wang, N. Xu, Y. Liu, and X. Zhao, "Adaptive fault-tolerant control for switched nonlinear systems based on command filter technique," *Appl. Math. Comput.*, vol. 392, Mar. 2021, Art. no. 125725.

[23] B. Sinopoli, L. Schenato, M. Franceschetti, K. Poolla, M. I. Jordan, and S. S. Sastry, "Kalman filtering with intermittent observations," *IEEE Trans. Autom. Control*, vol. 49, no. 9, pp. 1453–1464, Sep. 2004.

[24] C. Yang, J. Zheng, X. Ren, W. Yang, H. Shi, and L. Shi, "Multi-sensor Kalman filtering with intermittent measurements," *IEEE Trans. Autom. Control*, vol. 63, no. 3, pp. 797–804, Mar. 2018.

[25] S. Gururajan, M. L. Fravolini, A. Rhudy, A. Moschitta, and M. Napolitano, "Evaluation of sensor failure detection, identification and accommodation (SFDIA) performance following common-mode failures of pitot tubes," SAE Tech. Paper 2014-01-2164, Sep. 2014.

[26] M. B. Rhudy, M. L. Fravolini, Y. Gu, M. R. Napolitano, S. Gururajan, and H. Chao, "Aircraft model-independent airspeed estimation without pitot tube measurements," *IEEE Trans. Aerosp. Electron. Syst.*, vol. 51, no. 3, pp. 1980–1995, Jul. 2015.

[27] X. Wang and E. E. Yaz, "Second-order fault tolerant extended Kalman filter for discrete time nonlinear systems," *IEEE Trans. Autom. Control*, vol. 64, no. 12, pp. 5086–5093, Dec. 2019.

[28] S. J. Julier and J. K. Uhlmann, "New extension of the Kalman filter to nonlinear systems," *Proc. SPIE*, vol. 3068, pp. 182–193, Apr. 1997.

[29] J. Bae, S. Yoon, and Y. Kim, "Fault-tolerant attitude estimation for satellite using federated unscented Kalman filter," in *Advances in Spacecraft Technologies*. Feb. 2011, pp. 213–232.

[30] L. Li and Y. Xia, "Stochastic stability of the unscented Kalman filter with intermittent observations," *Automatica*, vol. 48, no. 5, pp. 978–981, May 2012.

[31] E. Naderi, N. Meskin, and K. Khorasani, "Nonlinear fault diagnosis of jet engines by using a multiple model-based approach," *J. Eng. Gas Turbines Power*, vol. 134, no. 1, pp. 1–10, Jan. 2012.

[32] D.-J. Lee, "Nonlinear estimation and multiple sensor fusion using unscented information filtering," *IEEE Signal Process. Lett.*, vol. 15, pp. 861–864, Dec. 2008.

[33] H. Y. Zhang, Y. L. Wang, and K. W. Du, "Robust detection filter design for jet engine control system," *IFAC Proc. Volumes*, vol. 24, no. 6, pp. 479–483, Sep. 1991.

[34] Y. Chen, F. Liu, S. Mei, and J. Ma, "A robust WLAV state estimation using optimal transformations," *IEEE Trans. Power Syst.*, vol. 30, no. 4, pp. 2190–2191, Jul. 2015.

[35] Y. Chen, J. Ma, P. Zhang, F. Liu, and S. Mei, "Robust state estimator based on maximum exponential absolute value," *IEEE Trans. Smart Grid*, vol. 8, no. 4, pp. 1537–1544, Jul. 2017.

[36] X.-H. Chang and G.-H. Yang, "Nonfragile H_∞ filtering of continuous-time fuzzy systems," *IEEE Trans. Signal Process.*, vol. 59, no. 4, pp. 1528–1538, Apr. 2011.

[37] X.-H. Chang, Q. Liu, Y.-M. Wang, and J. Xiong, "Fuzzy peak-to-peak filtering for networked nonlinear systems with multipath data packet dropouts," *IEEE Trans. Fuzzy Syst.*, vol. 27, no. 3, pp. 436–446, Mar. 2019.

TONGPAN NIE received the B.S. degree in electrical engineering from Chongqing University, Chongqing, China, in 2001. He joined the Testability Department of The First Aircraft Institute (FAI) of the Aviation Industry Corporation of China (AVIC) in 2001. He is currently the Chief Designer of the Prognostic and Health Management (PHM) Department, FAI. His research interests include aircraft PHM, avionics software, and system engineering.

YU WANG received the B.S. and M.S. degrees from Northwestern Polytechnical University, in 2003 and 2006, respectively. He is currently a Senior Engineer with the Department of Propulsion System, FAI. His research interests include the design and validation of aircraft propulsion and fire protection systems.

ZIYU DENG received the B.S. degree in mechatronics from Northwestern Polytechnical University, Xi'an, China, in 2020, where he is currently pursuing the master's degree with the School of Mechanical Engineering. He is in the internship program of the First Aircraft Institute. His research interests include state estimation, control engineering, and aircraft PHM.

XIANSHENG QIN received the B.S., M.S., and Ph.D. degrees in aerospace manufacturing engineering from the Northwestern Polytechnical University (NPU), Xi'an, China, in 1983, 1986, and 1991, respectively. He is currently a Professor with the School of Mechanical Engineering, NPU, and the Director of the NPU–Xi'an Aircraft Corporation Center of Aviation Manufacturing Systems. He received the AVIC Science Progress Award from the Aviation Industry Corporation of China in 1998, and the Rong Hong Award from the United Technologies (now Raytheon Technologies) in 1999. For over three decades, he has been focused on solving the real-world problems in aerospace manufacturing, mechatronics, and system engineering.

• • •